



Contents lists available at ScienceDirect

Translational Oncology

journal homepage: www.elsevier.com/locate/tranon

Loss of S6K1 But Not S6K2 in the Tumor Microenvironment Suppresses Tumor Growth by Attenuating Tumor Angiogenesis



Seul Lee ^{a,1}, Hyun-Soo Roh ^{a,1}, Seong-Soo Song ^a, Jimin Shin ^a, Jangchoon Lee ^a, Dong Ha Bhang ^a, Byung Gak Kim ^a, Sung Hee Um ^a, Han-Sin Jeong ^{b,*}, Kwan-Hyuck Baek ^{a,*}

^a Department of Molecular and Cellular Biology, Sungkyunkwan University School of Medicine, Suwon, Gyeonggi 16419, Republic of Korea

^b Department of Otorhinolaryngology-Head and Neck Surgery, Samsung Medical Center, Sungkyunkwan University School of Medicine, Seoul 06351, Republic of Korea

ARTICLE INFO

Article history:

Received 28 January 2020

Accepted 17 March 2020

Available online xxxx

ABSTRACT

Two isoforms of the 70-kDa ribosomal protein S6 kinase, S6K1 and S6K2, have been identified and are considered key downstream effectors of the mTOR signaling pathway, which is involved in tumor growth and progression. However, their biological roles in the tumor microenvironment are poorly understood. In this study, utilizing tumor xenograft models in *S6k1*^{-/-} and *S6k2*^{-/-} mice, we show that loss of S6K1 but not S6K2 in the tumor stroma suppresses tumor growth, accompanied by attenuated tumor angiogenesis. We found that while S6K1 depletion had no effect on the proangiogenic phenotype of endothelial cells, the growth and angiogenesis of tumor xenografts were significantly reduced in wild-type mice upon reconstitution with S6K1-deficient bone marrow cells. Furthermore, upon S6K1 loss, induction of both mRNA and protein levels of *Hif-1α* and those of the downstream target, *Vegf*, was compromised in bone marrow-derived macrophages stimulated with lactate. These findings indicate that S6K1 but not S6K2 contributes to establishing a microenvironment that favors tumor growth through mediating angiogenesis, and suggest that attenuated tumor angiogenesis upon loss of S6K1 in the tumor stroma is, at least in part, attributable to impaired upregulation of *Vegf* in tumor-associated macrophages.

© 2020 The Authors. Published by Elsevier Inc. on behalf of Neoplasia Press, Inc. This is an open access article under the CC BY-NC-ND license (<http://creativecommons.org/licenses/by-nc-nd/4.0/>).

Introduction

Interactions between tumor cells and their surrounding microenvironment are crucial for tumorigenesis [1]. Indeed, many cellular and molecular factors in the tumor stroma, including fibroblasts, immune cells, endothelial cells, cytokines, chemokines, growth factors, and extracellular matrix, have been identified and shown to contribute to tumor growth and progression through angiogenesis, immune evasion, extracellular matrix remodeling, and metastasis [2,3]. Therefore, delineation of signaling networks involved in conferring the microenvironment with tumor-promoting properties is essential for fully understanding tumorigenesis and has significant clinical implications.

Mammalian target of rapamycin (mTOR), a serine/threonine kinase belonging to the phosphatidylinositol-3-OH kinase-related kinase family, is a

* Address all correspondence to: Kwan-Hyuck Baek, PhD, Department of Molecular and Cellular Biology, Sungkyunkwan University School of Medicine, 2066 Seobu-ro, Jangan-gu, Suwon, Gyeonggi 16419, Republic of Korea. or Han-Sin Jeong, M.D., Ph.D. Department of Otorhinolaryngology-Head and Neck Surgery, Samsung Medical Center, Sungkyunkwan University School of Medicine, 81 Irwon-ro, Gangnam-gu, Seoul 06351, Republic of Korea.

E-mail addresses: hansin.jeong@samsung.com, (H.-S. Jeong), khbaek@skku.edu (K.-H. Baek).

¹ These authors contributed equally to this work.

master regulator in signal transduction pathways coupling mitogenic and nutrient stimuli to cell proliferation, survival, motility, and metabolism [4]. Extensive studies on mTOR have revealed its fundamental roles in the control of various cellular processes including protein synthesis and turnover, as well as its contribution to tumor growth and progression through altering translational and metabolic landscapes in tumor cells [4–6]. Indeed, deregulated mTOR signaling is frequently observed in many types of human cancer cells, supporting its pivotal role in tumorigenesis in a tumor cell-intrinsic manner [4–6]. In addition, accumulating evidence indicates that mTOR signaling is involved in regulating the tumor-promoting behaviors of various types of cells other than tumor cells within the tumor microenvironment, such as tumor-associated fibroblasts (TAFs), endothelial cells, myeloid-derived suppressor cells (MDSCs), tumor-associated macrophages (TAMs), and regulatory T cells, suggesting that mTOR signaling contributes to tumor growth and progression not only in a tumor cell-intrinsic manner but also in a tumor cell-extrinsic manner [7]. However, despite the emerging roles of mTOR in the tumor microenvironment, its downstream signaling pathways are poorly elucidated.

The 70-kDa ribosomal protein S6 kinase (S6K) is a major downstream effector of mTOR [8]. Upon activation by mTOR-dependent phosphorylation, S6K enhances protein synthesis from mRNA templates by promoting translational initiation and elongation through phosphorylation of its

targets, including eukaryotic translation initiation factor 4B, eukaryotic elongation factor kinase, and 40S ribosomal protein S6, thereby contributing to mTOR-mediated translation control of gene expression in response to mitogenic and nutrient stimuli [8]. In addition, S6K mediates metabolic shifts triggered by mTOR activation via direct regulation of metabolic enzymes as well as activation of key metabolic transcription factors such as hypoxia-inducible factors (HIFs) and sterol regulatory element binding proteins [9–11]. Recent studies have shown that S6K also participates in regulation of gene expression at the transcriptional level by modifying histone proteins or recruiting transcriptional corepressors to the nucleus [12,13], suggesting that S6K mediates mTOR signaling through both translation-dependent and -independent mechanisms. While extensive research has delineated the functions of S6K in mediating mTOR signaling in tumor cells [14], only a few studies have reported the downstream role of S6K1 in the tumor stroma [15,16]; thus, its contribution to the tumor microenvironment remains unclear.

Two isoforms of S6K, S6K1 and S6K2, have been identified and are considered to have redundant functions based on significant sequence homology in their catalytic domains and ubiquitous expression of their mRNAs in all mouse and human tissues examined [8,14]. However, recent studies have revealed differences in subcellular localization, upstream regulation, and downstream targets of these isoforms [14]. In addition, *S6k1*^{-/-} and *S6k2*^{-/-} mice were found to exhibit distinct patterns of embryonic development [17]. This evidence suggests that each S6K isoform has a distinct role in tumorigenesis. Indeed, S6K1 but not S6K2 was reported to be essential for insulinoma formation triggered by constitutively active Akt1 expression in the mouse pancreas [18]. However, little is known about the roles of the two S6K isoforms in mTOR signaling with regard to establishment of a tumor microenvironment. Therefore, in this study, we examined the effect of loss of each isoform from the tumor stroma on tumor growth and addressed the underlying cellular and molecular mechanisms utilizing xenograft tumor models in genetically engineered mice with either *S6k1* or *S6k2* deleted.

Materials and Methods

Mice

S6k1^{-/-} and *S6k2*^{-/-} mice with a C57BL/6 background were a kind gift from Dr. Sara Kozma and Dr. George Thomas (University of Cincinnati). Green fluorescent protein (*Gfp*)-transgenic mice on a C57BL/6 background were kindly provided by Dr. Jae Hyeon Kim (Samsung Medical Center, Sungkyunkwan University School of Medicine). Wild-type C57BL/6 mice were obtained from Jackson Laboratories. To generate *Gfp* mice knockouts of either *S6k1* or *S6k2*, *Gfp* mice were crossed with *S6k1*^{-/-} and *S6k2*^{-/-} mice, and their genotypes were determined by polymerase chain reaction (PCR) analysis of genomic DNA isolated from toe biopsies as described previously [17,19,20].

All animal studies were approved by the Institutional Animal Care and Use Committee of Sungkyunkwan University School of Medicine and performed at the Laboratory Animal Research Center of Sungkyunkwan University School of Medicine (permit no. 001004). The Laboratory Animal Research Center is a registered research facility with the Association for Assessment and Accreditation of Laboratory Animal Care International and is committed to complying with the guide for the care and use of laboratory animals of the National Research Council of the United States.

Cell Lines

The B16F10 melanoma cell line was purchased from American Type Culture Collection. The Lewis lung carcinoma (LLC) cell line was a kind gift from Dr. Sandra Ryeom (Perelman School of Medicine at the University of Pennsylvania). Tumor cell lines were grown in DMEM medium (WelGENE) supplemented with 10% fetal bovine serum (FBS, Gemini Bio-Products), 2 mM L-glutamine, 50 U/ml penicillin, and 50 µg/ml streptomycin (WelGENE). The murine fibroblast cell line L929 was obtained from the

American Type Culture Collection and cultured in RPMI-1640 medium containing 10% FBS, 2 mM L-glutamine, 50 U/ml penicillin, and 50 µg/ml streptomycin. All cell lines were maintained at 37°C in a humidified atmosphere of 5% CO₂.

Tumor Xenografts Studies

A total of 5 × 10⁵ LLC or B16F10 cells resuspended in 100-µl phosphate-buffered saline (PBS, Sigma) were inoculated subcutaneously into 6- to 8-week-old *S6k1*^{-/-}, *S6k2*^{-/-}, and wild-type male mice. Growth of tumors was then monitored by measuring tumor volume using digital calipers every 3 or 5 days. To generate a tumor xenograft model in bone marrow-transferred mice, 10⁶ B16F10 cells in 100 µl PBS were injected into the subcutaneous region of recipient mice at 5 weeks after bone marrow transplantation. Diameters of implanted tumors were then measured with digital calipers every 3 or 4 days for 31 days after injection. Tumor volume was calculated as 0.52 × length × width² [21].

Immunohistochemistry

Mice were euthanized by CO₂ asphyxiation, and tumors were harvested and fixed in 10% neutral buffered formalin. Paraffin-embedded sections of tumors were prepared and immunostained with rabbit polyclonal anti-CD31 and mouse monoclonal anti-α-smooth muscle actin (α-SMA) antibodies (Abcam) followed by further incubation with goat anti-rabbit IgG Alexa 594 and goat anti-mouse IgG Alexa 488 antibodies (ThermoFisher Scientific) as described previously [22]. Sections were then counterstained with 0.5 µg/ml 4',6-diamidino-2-phenylindole (Sigma) to visualize cell nuclei, mounted, and examined under a fluorescence microscope (Carl Zeiss).

Microvessel density (MVD) and pericyte coverage were quantified in three to five randomly selected high-power fields per tumor. CD31-positive area, the area positive for both CD31 and α-SMA, and the total tumor area were measured using ImageJ software (National Institute of Health). MVD and pericyte coverage were then determined as a percentage of the CD31-positive area per field and a percentage of α-SMA-positive pericyte surface area covering the CD31-positive capillary surface area, respectively.

Primary Endothelial Cell Isolation

One- to 2-week-old mice were euthanized, the lungs removed, and primary endothelial cells isolated by sequential staining with FITC-conjugated rat monoclonal anti-ICAM-2 (Southern Biotech) and microbead-conjugated monoclonal anti-FITC (Miltenyi Biotec) antibodies followed by magnetic-activated cell sorting on MS columns (Miltenyi Biotec) as described previously [22]. Cells were then plated into a tissue culture flask (ThermoFisher Scientific) coated with 0.1% gelatin (Sigma) and grown in complete growth medium (advanced DMEM supplemented with 25 mM HEPES) (ThermoFisher Scientific), 100 µg/ml heparin (Sigma), 100 µg/ml endothelial cell growth supplement (ECGS, Biomedical Technologies), 20% FBS, 2 mM L-glutamine, 50 U/ml penicillin, and 50 µg/ml streptomycin. The purity of isolated endothelial cells was determined using immunostaining for CD31 followed by examination under a confocal microscope (Carl Zeiss), and cells between passages 2 and 6 were used for experiments.

Cell Proliferation

A total of 2.5 × 10⁴ primary endothelial cells were seeded in triplicate in 12-well tissue culture plates (ThermoFisher Scientific) coated with 0.1% gelatin, incubated in complete growth media, and counted every 24 hours for 3 days using the Multisizer 4 Coulter Counter (Beckman Coulter). For VEGF-induced endothelial cell proliferation, 2.5 × 10⁴ primary endothelial cells were plated in triplicate in 12-well tissue culture plates, serum-starved in Advanced DMEM supplemented with 2% FBS for 24 hours, and further incubated in starvation medium containing 50 ng/ml VEGF (BioLegend). Cells maintained in starvation medium alone were used as the negative

control. After 72 hours of VEGF treatment, cells were counted using the Coulter counter.

For 5-bromo-2'-deoxyuridine (BrdU) incorporation assays, 7.5×10^3 primary endothelial cells were plated on gelatin-coated 12-mm coverslips (Neuvitro Corporation), incubated overnight, and grown in complete growth medium for 48 hours. Cells were also incubated overnight, serum-starved for 24 hours, and treated with 50 ng/ml VEGF for 48 hours. Cells were then pulsed with 10 μ M BrdU (Sigma) for 1 hour and probed with rat monoclonal anti-BrdU (Abcam) and anti-CD31 antibodies followed by incubation with goat anti-rat IgG Alexa 594 and goat anti-rabbit IgG Alexa 488 antibodies (ThermoFisher Scientific) to detect BrdU uptake and to identify endothelial cells, respectively [23]. Cells were then counter-stained with 0.5 μ g/ml 4',6-diamidino-2-phenylindole, and BrdU-positive endothelial cells were quantified using TissueFAXS scanning and TissueQuest analysis software (TissueGnostics GmbH).

Tube Formation Assay

A total of 3×10^4 primary endothelial cells were resuspended in 100 μ l OPTI-MEM (ThermoFisher Scientific) supplemented with 1% FBS, seeded in triplicate in 96-well tissue culture plates (ThermoFisher Scientific) coated with 100 μ l of standard Matrigel (BD Biosciences), and incubated for 12 hours at 37°C in a CO₂ incubator. Images were then acquired from three different fields in each well using an inverted bright-field microscope (Nikon), and total tube lengths were measured using ImageJ software.

Apoptosis Assay

A total of 3×10^5 primary endothelial cells were plated in triplicate in a six-well tissue culture plate (ThermoFisher Scientific) coated with 0.1% gelatin and grown overnight. Cells were then incubated in starvation medium containing 50 ng/ml VEGF or starvation medium alone as a control. After 72 hours, cells were harvested and apoptotic cells were stained using the APC Annexin-V apoptosis detection kit (BD Biosciences) according to the manufacturer's instructions. Apoptotic cells were then quantified by flow cytometry using a FACS Canto II flow cytometer (Becton Dickinson).

Matrigel Plug Assay

Growth factor-reduced Matrigel (BD Biosciences) was mixed with 0.1 mg/ml heparin (Sigma), 200 ng/ml VEGF, and 600 ng/ml basic fibroblast growth factor (bFGF, BioLegend), and 300 μ l of the Matrigel mixture was inoculated subcutaneously into the right flank of 6- to 8-week-old mice. The same volume of Matrigel combined with 0.1 mg/ml heparin only was also injected into the subcutaneous region of the left flank of the mice as a control. At 7 days postinjection, Matrigel plugs were harvested from the mice, fixed in 10% formalin in PBS, embedded in paraffin, sectioned, stained for CD31 and α -SMA, and analyzed as described above.

Bone Marrow Transplantation

Bone marrow transplantation was performed as described previously [24]. Briefly, 6-week-old recipient mice were irradiated twice with a lethal dose of 6.5 Gy from a ¹³⁷Cs source at 4-hour intervals. Eight- to 10-week-old donor mice were euthanized, and bone marrow cells were isolated from tibias and femurs by flushing the bones with sterile RPMI-1640 medium and straining the cells through a 40- μ m strainer. A total of 10^7 bone marrow cells from donor mice were then administered intravenously via the tail vein of irradiated recipient mice. After 5 weeks of recovery, recipient mice were injected subcutaneously with B16F10 cells, and the growth of implanted tumors was monitored as described above. At the end of the experiment, bone marrow reconstitution in recipient mice was verified by detecting GFP-positive cells in blood cells using flow cytometry.

Flow Cytometry

Mice bearing B16F10 and LLC tumors approximately 1000 mm³ in volume were euthanized, and mononuclear cells were isolated from peripheral blood collected via eye bleeding and from the bone marrow obtained by flushing femurs. A single cell suspension of the tumors was prepared by mincing the tumors with a razor blade, homogenizing them by mechanical disruption, and incubating the homogenized tissue in 1 mg/ml of collagenase/dispase (Roche) and DNase I (Sigma) in RPMI-1640 medium as described previously [25]. Red blood cells were removed by incubation in ammonium-chloride-potassium (ACK) lysis buffer (ThermoFisher Scientific), and cells were incubated with 1 μ g of anti-mouse CD16/32 antibody (eBioscience) per 10^6 cells to block Fc receptors. Cells were then stained with PE-conjugated anti-mouse Gr-1 (1:200), FITC-conjugated anti-mouse CD11b (1:100), PE-conjugated anti-mouse F4/80 (1:100, eBioscience), and FITC-conjugated anti-mouse CD206 (1:50, BioLegend) antibodies. Before data acquisition on a FACS Canto II cytometer and analysis using FlowJo software (Tree Star), dead cells were excluded from all samples by staining with the Live/Dead Fixable Far Red Dead Cell Stain kit (ThermoFisher Scientific) following the manufacturer's instructions.

Bone Marrow-Derived Macrophage Preparation

To prepare L929 cell-conditioned media containing macrophage colony-stimulating factor, 2.4×10^5 L929 cells were seeded in a 150-mm tissue culture plate and grown in 25 ml of RPMI-1640 medium supplemented with 10 mM HEPES, 10% FBS, 2 mM L-glutamine, 50 U/ml penicillin, and 50 μ g/ml streptomycin for 1 week. Conditioned media were removed and replaced with fresh media every 7 to 8 days for 2 weeks. Collected media were then mixed at a 1:1 ratio, filtered through a 0.22- μ m filter, aliquoted, and stored at -80°C until use.

Bone marrow-derived macrophages (BMDMs) were prepared as described previously [26]. Briefly, 8- to 12-week old mice were euthanized, and bone marrow cells were harvested by flushing tibias and femurs with sterile RPMI-1640 medium. Red blood cells were lysed using ACK lysis buffer, and cells were plated on a 90-mm Petri dish (ThermoFisher Scientific) and allowed to differentiate into macrophages in RPMI-1640 medium supplemented with 10 mM HEPES, 15% FBS, 20% L929 cell-conditioned media, 2 mM L-glutamine, 50 U/ml penicillin, and 50 μ g/ml streptomycin for 1 week and then used for experiments.

Enzyme-linked immunosorbent assay (ELISA)

To measure intratumoral Bv8 concentration, B16F10 and LLC tumor xenografts approximately 1000 mm³ in volume were harvested from mice, minced into 1-mm³ pieces, and lysed in radioimmunoprecipitation assay buffer supplemented with 10 mM NaF, 1 mM Na₃VO₄, 1 μ M DTT, 1 mM PMSF (Sigma), and protease inhibitor cocktail (Roche). The concentration of Bv8 in tumor lysates was then measured using the mouse Prokineticin-2 ELISA kit (MyBioSource) according to the manufacturer's instruction and normalized to the total protein amount in the lysates.

To detect VEGF production in bone marrow-derived macrophages, 2.5×10^5 macrophages were seeded in hexuplicate in a 24-well tissue culture plate (ThermoFisher Scientific); grown overnight; serum starved in RPMI-1640 medium containing 1% FBS for 24 hours; and treated with 10 mM lactate, 100 μ g/ml lipopolysaccharide (LPS) combined with 1 μ M 5'-N-ethylcarboxamidoadenosine (NECA), or starvation media alone as a control for 24 hours. Supernatants were then removed and assessed for VEGF concentration using the mouse VEGF Quantikine ELISA kit (R&D Systems) according to the manufacturer's instructions.

2.14. Real-Time PCR

A total of 2×10^6 BMDMs were plated in 60-mm tissue culture plates (ThermoFisher Scientific), grown overnight, serum starved for 24 hours, and treated with 10 mM lactate or starvation medium only as a control

for 4 and 6 hours. Macrophages were then lysed with TRIZOL reagent (QIAGEN), and total RNA was purified using RNeasy columns (QIAGEN) according to the manufacturer's instructions. One microgram of total RNA was reverse transcribed to cDNA using the ImProm-II Reverse Transcription System (Promega) following the manufacturer's instructions. Quantitative real-time PCR was then performed on a QuantStudio 6 Flex Real-Time PCR System (Applied Biosystems) using Power SYBR Green PCR master mix (Applied Biosystems). The following primers were used to quantify *Vegf* and *Hif-1 α* mRNAs in macrophages: murine *Vegf* forward 5'-CCA CGA CAG AAG GAG AGC AGA AGT CC-3', reverse 5'-CGT TAC AGC AGC CTG CAC AGC G-3'; murine *Hif-1 α* forward 5'-CAC CGA TTC GCC ATG GA-3', reverse 5'-TTT CTT TTC GAC GTT CAG AAC TCA T-3'; murine β -Actin forward 5'-CCC GCC ACC AGT TCG CC-3', reverse 5'-GAG GGA GAG CAT AGC CCT CG-3'.

Immunoblotting

A total of 2×10^6 BMDMs were plated in 60-mm tissue culture plates, grown overnight, serum-starved for 24 hours, and treated with 10 mM lactate for 4 and 6 hours. As an untreated control, macrophages were also incubated in starvation medium alone for 6 hours. Macrophages were harvested, lysed, separated on SDS-PAGE, and probed for HIF-1 α (Bethyl Laboratories, Montgomery, TX) and β -actin (Sigma) as a loading control. Band intensities were quantified by densitometric analysis using ImageJ software, and relative gel densities were determined by normalizing to β -actin as described previously [27].

Statistical Analysis

Two-tailed unpaired Student's *t* tests were used to determine the statistical significance of differences between groups, and *P* values less than .05 were considered to indicate a statistically significant difference.

Results

Loss of S6K1 But Not S6K2 in the Tumor Microenvironment Reduces Tumor Growth by Attenuating Tumor Angiogenesis

To explore the role of each S6K isoform in the tumor microenvironment during tumorigenesis, we investigated the growth of B16F10 and LLC xenografts in *S6k1*^{-/-} and *S6k2*^{-/-} mice (Figure 1). While the growth of both B16F10 and LLC xenografts in *S6k2*^{-/-} mice was comparable to that of tumors implanted in wild-type controls, xenograft growth was significantly suppressed in *S6k1*^{-/-} mice, resulting in a dramatic decrease in tumor volume and weight by around 60% compared to tumors in control mice at days 20 and 25, respectively, after subcutaneous injection (Figure 1, A-D). These observations suggest that S6K1 but not S6K2 is required to establish a tumor-promoting microenvironment.

Therapeutic inhibition of mTOR has been shown to restrain tumor growth through attenuating tumor angiogenesis as well as abrogating tumor cell proliferation [28]. To investigate the mechanism underlying the suppression of tumor growth observed in S6K1-deficient tumor stroma, we assessed MVD in B16F10 and LLC tumor xenografts from *S6k1*^{-/-} and *S6k2*^{-/-} mice as well as wild-type controls using immunostaining for

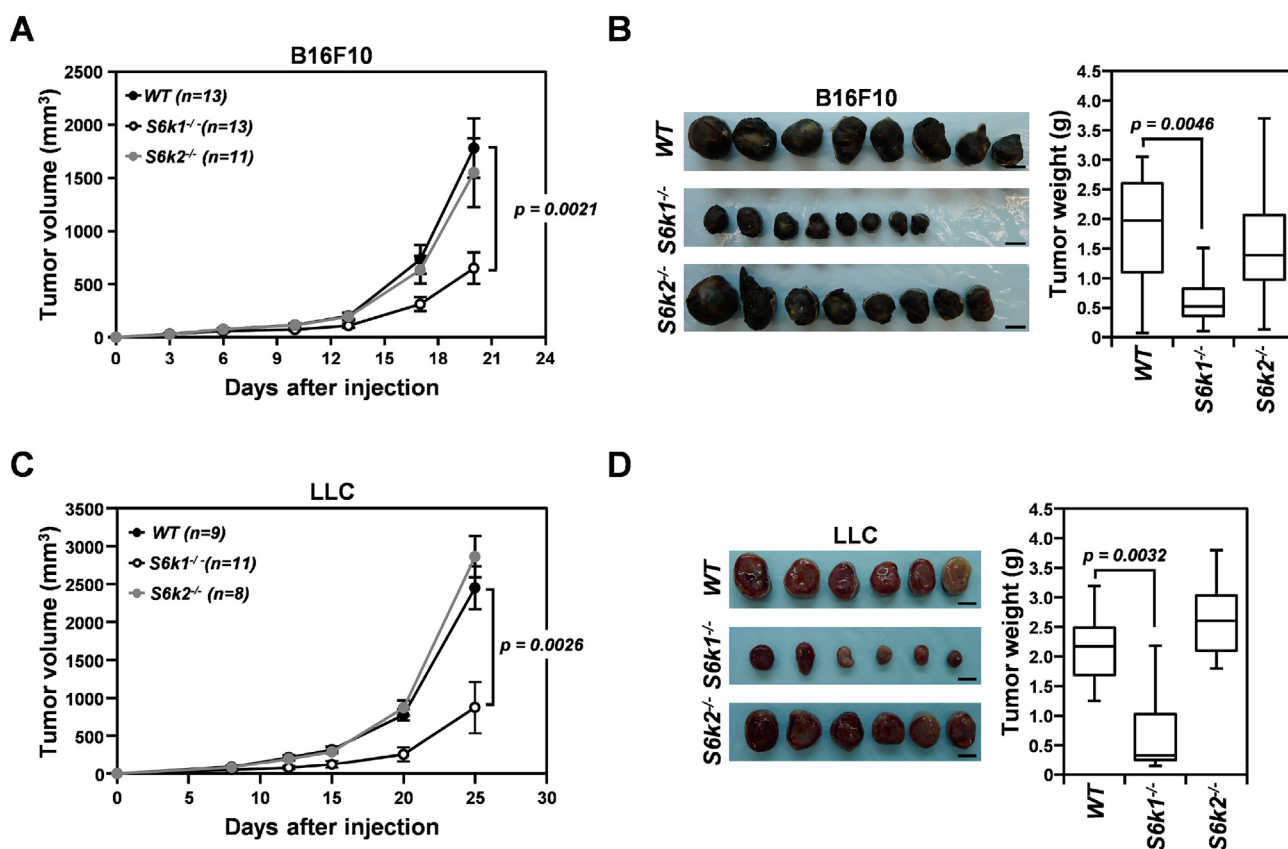


Figure 1. Loss of S6K1 but not S6K2 in the tumor stroma suppresses the growth of implanted tumors. (A) Growth curves of B16F10 xenografts in *S6k1*^{-/-}, *S6k2*^{-/-}, and wild-type mice. (B) Representative images (left panel) and weights (right panel) of B16F10 tumors harvested from *S6k1*^{-/-}, *S6k2*^{-/-}, and wild-type mice at 20 days postinjection. (C) Growth curves of LLC xenografts in *S6k1*^{-/-}, *S6k2*^{-/-}, and wild-type mice. (D) Representative images (left panel) and weights (right panel) of LLC tumors isolated from *S6k1*^{-/-}, *S6k2*^{-/-}, and wild-type mice at 25 days after injection. Scale bars: 1 cm. Data are presented as means \pm standard errors of the mean (SEM) for tumor growth curves and box plots with median values for tumor weights.

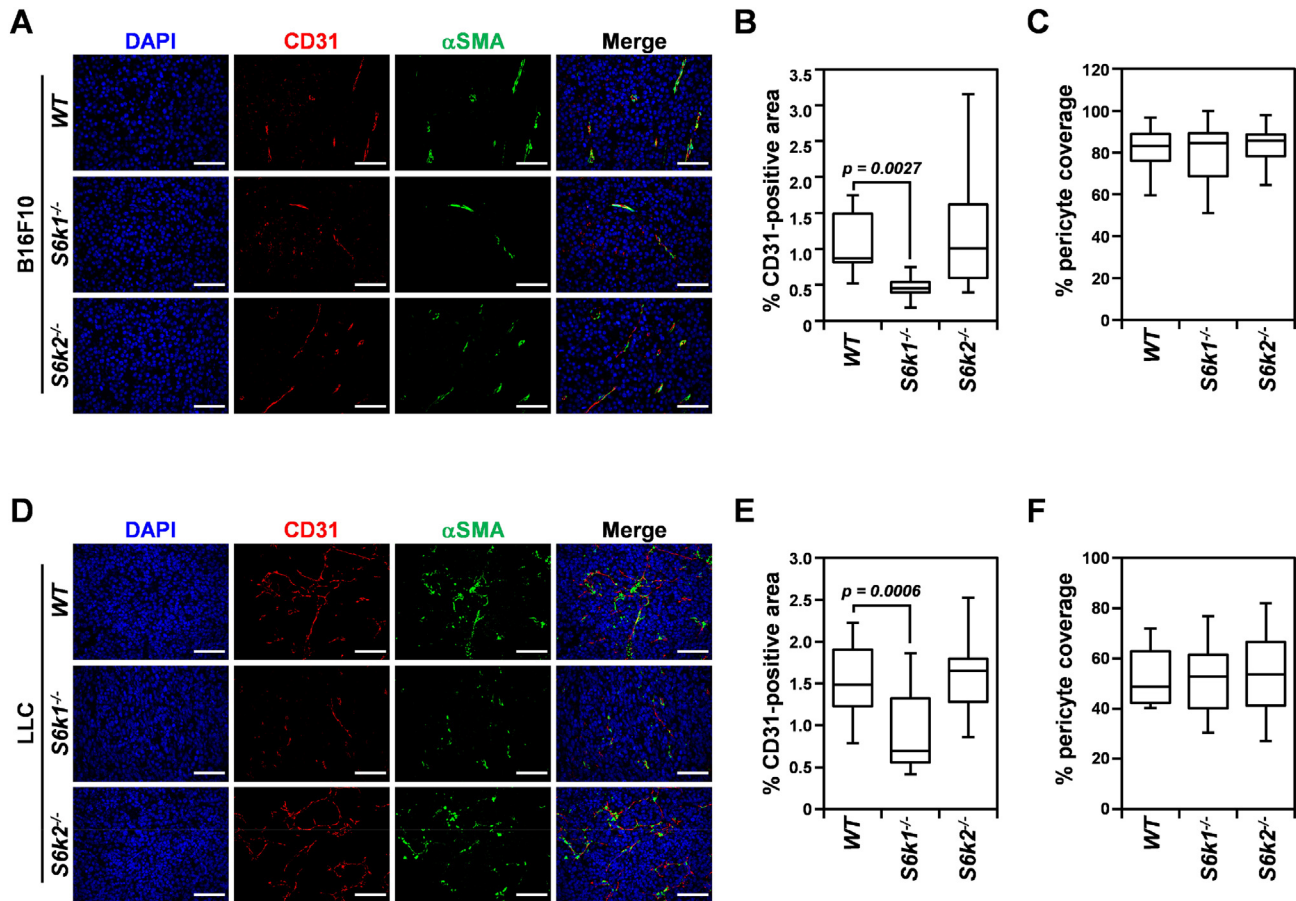


Figure 2. Tumor angiogenesis is attenuated in the S6K1-deficient but not S6K2-deficient tumor microenvironment. (A–C) Representative images of immunostaining for CD31 and α -SMA (A) and quantification of MVD (B) and pericyte coverage of CD31-positive vessels (C) in B16F10 xenografts isolated from *S6k1*^{-/-}, *S6k2*^{-/-}, and wild-type mice at 20 days postinjection. (D–F) Representative images of immunostaining for CD31 and α -SMA (D) and quantification of MVD (E) and pericyte coverage of CD31-positive vessels (F) in LLC tumors harvested from *S6k1*^{-/-}, *S6k2*^{-/-}, and wild-type mice at 25 days after injection. Scale bars: 50 μ m. Data are presented as box plots with medians and min to max whiskers.

CD31, an endothelial cell marker (Figure 2). In parallel with tumor growth, the mean CD31-positive area was significantly reduced in both B16F10 and LLC xenografts from *S6k1*^{-/-} but not from *S6k2*^{-/-} mice by up to 50% and 41%, respectively, compared to wild-type controls (Figure 2, A, B, D, and E). These data suggest that the suppression of tumor growth observed in *S6k1*^{-/-} mice is, at least in part, due to impaired angiogenesis in the absence of S6K1-mediated signaling in the tumor stroma, lending support to our hypothesis that S6K1 but not S6K2 is essential for creating a microenvironment that favors tumor growth.

Coverage of the neovasculature by pericytes is crucial for vessel maturation and stability and thus is an important step in the angiogenic process [29]. In addition, a defect in pericyte coverage of the tumor vasculature has been shown to reduce tumor growth [30]. Therefore, we also investigated how loss of each S6K isoform affected the recruitment of pericytes to the tumor vasculature (Figure 2, A, C, D, and F). Assessment of the CD31-positive area covered by pericytes using immunostaining for α -SMA, a pericyte marker, revealed that the α -SMA-positive area of tumor microvessels in both B16F10 and LLC tumors remained unchanged in the absence of either S6K1 or S6K2 compared to wild-type controls, suggesting that loss of S6K1 in the tumor stroma attenuates tumor angiogenesis without affecting pericyte coverage.

Loss of S6K Isoforms Does Not Attenuate the Angiogenic Activity of Endothelial Cells Either In Vitro or In Vivo

mTOR inhibition has been shown to dampen proangiogenic activation of endothelial cells, which are major players in tumor

angiogenesis [28]. Therefore, we examined whether loss of S6K isoforms, especially S6K1, interfered with endothelial activation and thus resulted in attenuated tumor angiogenesis in our mouse tumor xenograft models. We first isolated primary endothelial cells from *S6k1*^{-/-}, *S6k2*^{-/-}, and wild-type mice and confirmed the expression of S6K isoforms in those cells by immunoblotting (Figure S1). We then examined the effect of loss of S6K isoforms on the angiogenic phenotypes of endothelial cells *in vitro* (Figure 3). Proliferation of wild-type endothelial cells grown in complete growth medium as assessed by both cell counting and BrdU incorporation was not significantly different from that of endothelial cells deficient for each S6K isoform (Figure 3, A and B). To further investigate whether loss of individual S6K isoforms affected endothelial cell proliferation triggered by a specific proangiogenic factor, cell proliferation was also measured in *S6k1*^{-/-}, *S6k2*^{-/-}, and wild-type endothelial cells as a control after treatment with VEGF, a major angiogenic factor involved in tumor angiogenesis (Figure 3, C and D). Similar to endothelial cells grown in complete growth medium, neither S6K1 nor S6K2 deficiency resulted in any significant change in cell count or BrdU-positive cell population compared with wild-type endothelial cells after VEGF treatment. In addition, tubulogenic activity assessed by a tube formation assay revealed that loss of either S6K1 or S6K2 by endothelial cells did not impair their capillary tube forming potential compared to wild-type controls (Figure 3E). Furthermore, neither *S6k1*^{-/-} nor *S6k2*^{-/-} endothelial cells exhibited alterations in the cell population undergoing apoptosis upon serum depletion or cell survival facilitated by VEGF compared to wild-type controls (Figure 3F).

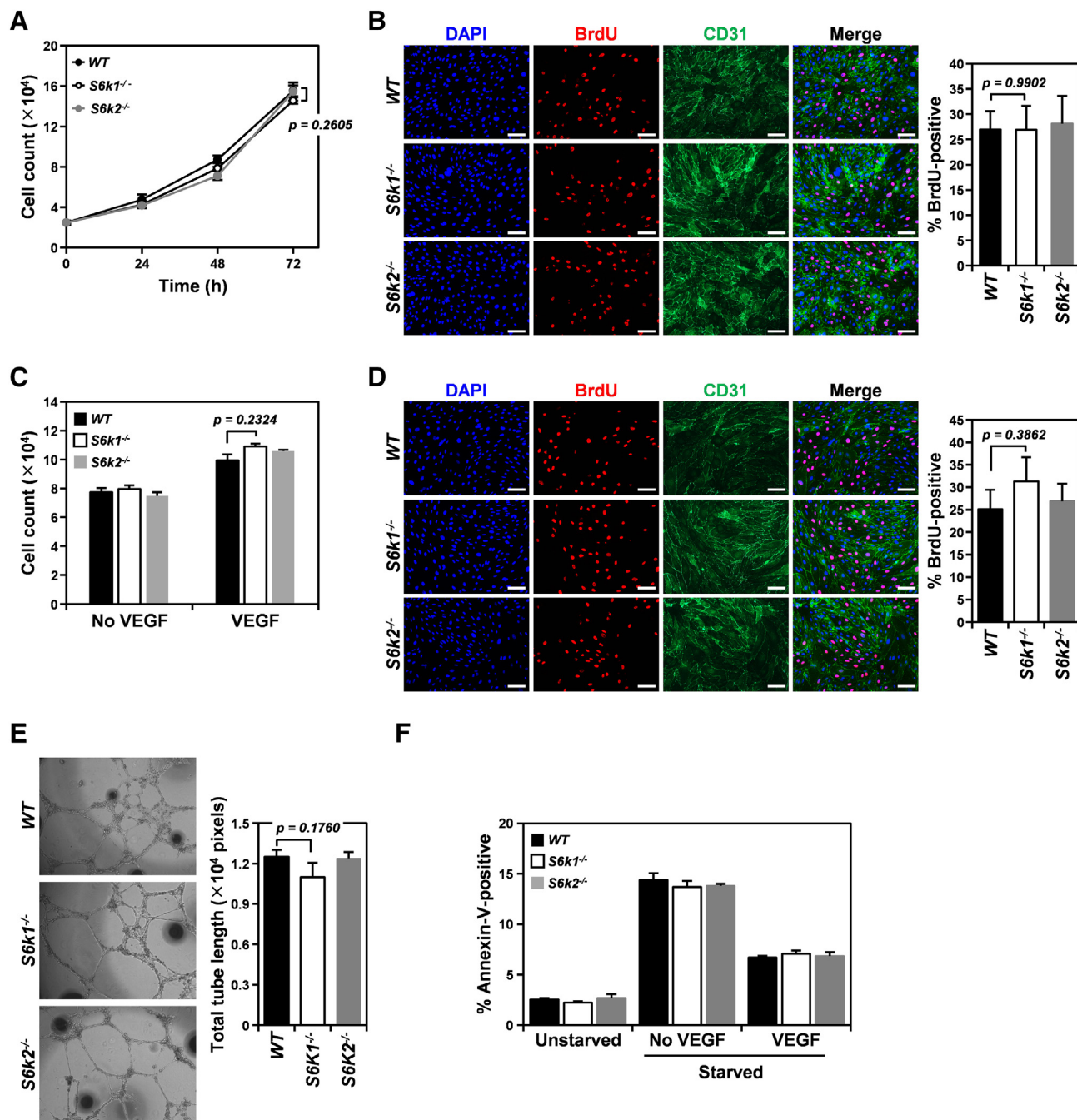


Figure 3. Loss of either S6K1 or S6K2 does not impair the angiogenic capacity of endothelial cells *in vitro*. (A and B) Cell proliferation assessed by cell count (A) and BrdU incorporation assay (B) in primary S6k1^{-/-}, S6k2^{-/-}, and wild-type endothelial cells grown in complete growth medium. (C and D) Cell proliferation measured by cell count (C) and BrdU incorporation assay (D) in primary S6k1^{-/-}, S6k2^{-/-}, and wild-type endothelial cells treated with 50 ng/ml VEGF for 72 and 48 hours, respectively. (E) Representative bright-field images of endothelial tube formation in S6k1^{-/-}, S6k2^{-/-}, and wild-type endothelial cells (left panel) and quantification of total tube length (right panel). (F) Apoptotic cell death assessed by staining for Annexin-V and flow cytometry analysis in S6k1^{-/-}, S6k2^{-/-}, and wild-type endothelial cells incubated in 50 ng/ml VEGF in starvation medium, starvation medium only, or complete growth medium as controls for 72 hours. Scale bars: 50 μ m. Data are presented as means \pm SEM.

To further verify our *in vitro* observations, we examined the effect of loss of S6K isoforms on endothelial cell invasion and microvessel formation induced by proangiogenic factors *in vivo* using a Matrigel plug assay (Figure 4). In all mice examined, a dramatic increase in blood influx and CD31-positive area was observed in Matrigel implants containing VEGF and bFGF compared to those mixed with heparin only as a negative control (Figure 4, A and B). However, neither S6k1^{-/-} nor S6k2^{-/-} mice had significant alterations in MVD in the Matrigel plugs compared to wild-type controls (Figure 4, B and

C). In addition, quantitation of the CD31-positive area covered by pericytes showed no defects in pericyte recruitment to newly formed blood vessels upon loss of S6K isoforms (Figure 4D), supporting our hypothesis that S6K signaling is dispensable for pericyte coverage of the tumor vasculature.

Taken together, our *in vitro* and *in vivo* data indicate that neither S6K1 nor S6K2 is necessary for proangiogenic activation of endothelial cells; thus, the suppressed tumor angiogenesis and growth observed in S6k1^{-/-} mice is not due to a defect in endothelial cells.

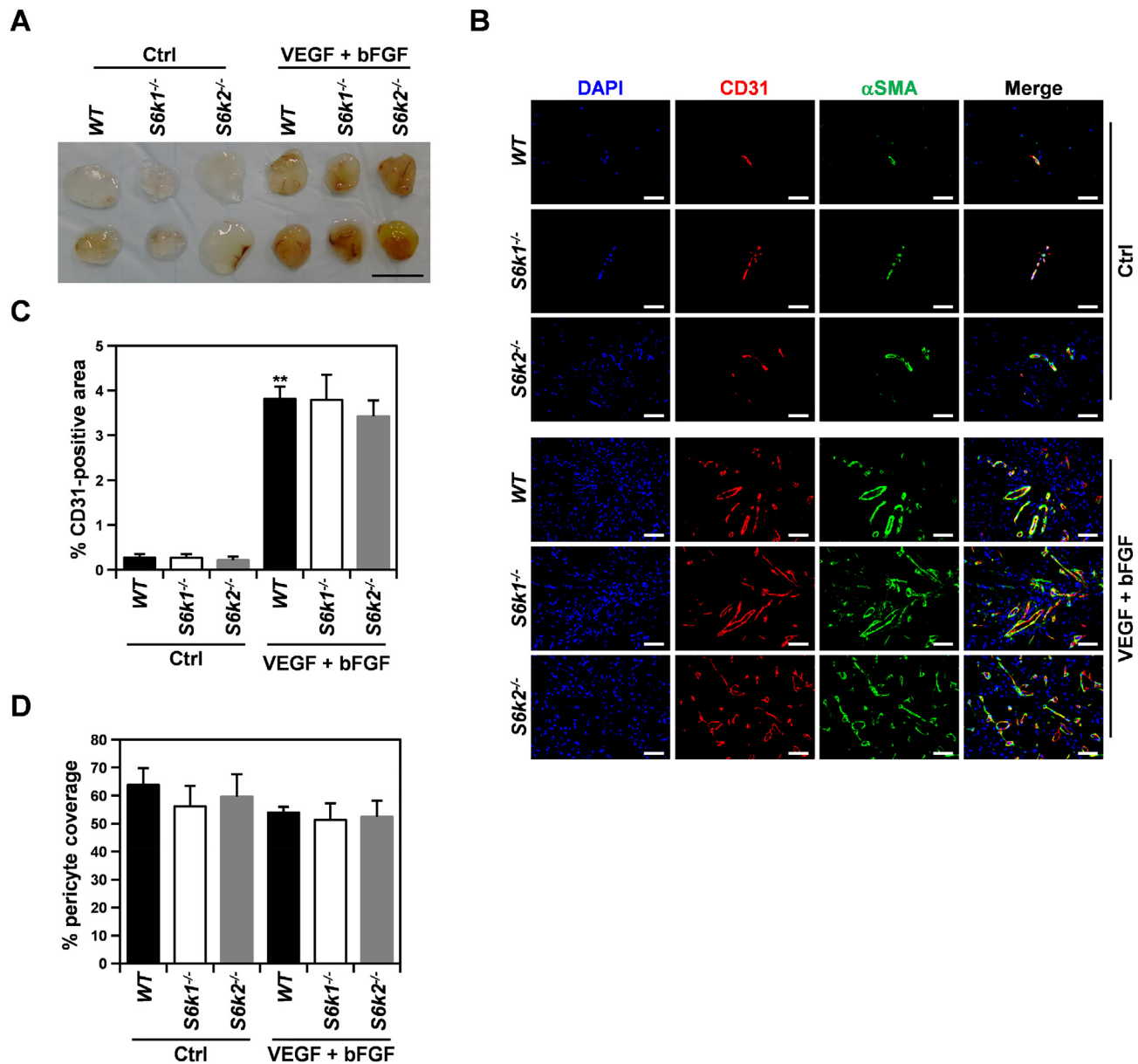


Figure 4. Loss of either S6K1 or S6K2 does not attenuate VEGF/bFGF-mediated angiogenesis *in vivo*. (A) Representative images of Matrigel implants containing a mixture of VEGF and bFGF or heparin only as a control (Ctrl) harvested from *S6k1*^{-/-} ($n = 5$), *S6k2*^{-/-} ($n = 5$), and wild-type ($n = 5$) mice at 7 days postinjection. Scale bars: 1 cm. (B) Representative immunofluorescence images of Matrigel plugs stained for CD31 and α -SMA. Scale bars: 50 μ m. (C and D) Quantification of MVD (C) and pericyte coverage of CD31-positive vessels (D) in the Matrigel implants. Data are presented as means \pm SEM. ** $P < 0.01$.

Loss of S6K1 But Not S6K2 in Bone Marrow-Derived Cells Results in Reduced Tumor Angiogenesis and Growth

Bone marrow-derived cells, especially immune cell subsets such as macrophages and MDSCs, are essential for initiating and driving tumor angiogenesis [3]. In addition, mTOR signaling has been shown to be required for the recruitment of immune cells to the tumor microenvironment as well as their differentiation and activation [7].

To identify cellular factors responsible for the attenuated tumor angiogenesis and growth observed in *S6k1*^{-/-} mice, we generated *Gfp* mice deficient for each S6K isoform, namely, *S6k1*^{-/-};*Gfp* and *S6k2*^{-/-};*Gfp* mice, transplanted bone marrow cells from those mice and wild-type *Gfp* mice as a control into lethally irradiated wild-type mice, and monitored the growth of B16F10 xenografts in the recipients (Figures 5 and S2). As expected, transplantation of *S6k2*^{-/-};*Gfp* bone

marrow cells did not impair the growth of B16F10 tumors compared to the wild-type control (Figure 5, A and B). However, similar to the tumor growth observed in *S6k1*^{-/-} mice (Figure 1), the growth of B16F10 xenografts was attenuated in mice that received bone marrow cells from *S6k1*^{-/-};*Gfp* donors, resulting in a significant reduction in the mean volume and weight of the tumors by 46% and 54% compared to those of wild-type controls at day 31 after subcutaneous injection (Figure 5, A and B). In addition, quantification of the CD31-positive area in xenografts revealed that MVD was significantly decreased (by around 60%) in B16F10 tumors implanted in mice reconstituted with *S6k1*^{-/-};*Gfp* bone marrow cells compared to that of wild-type recipient controls (Figure 5C). These observations indicate that the reduced tumor angiogenesis and growth observed in *S6k1*^{-/-} mice are, at least in part, due to an angiogenic defect in tumor-infiltrating bone marrow-derived cells, suggesting that S6K1 signaling is required for the angiogenic activity of tumor-infiltrating bone marrow-derived cells.

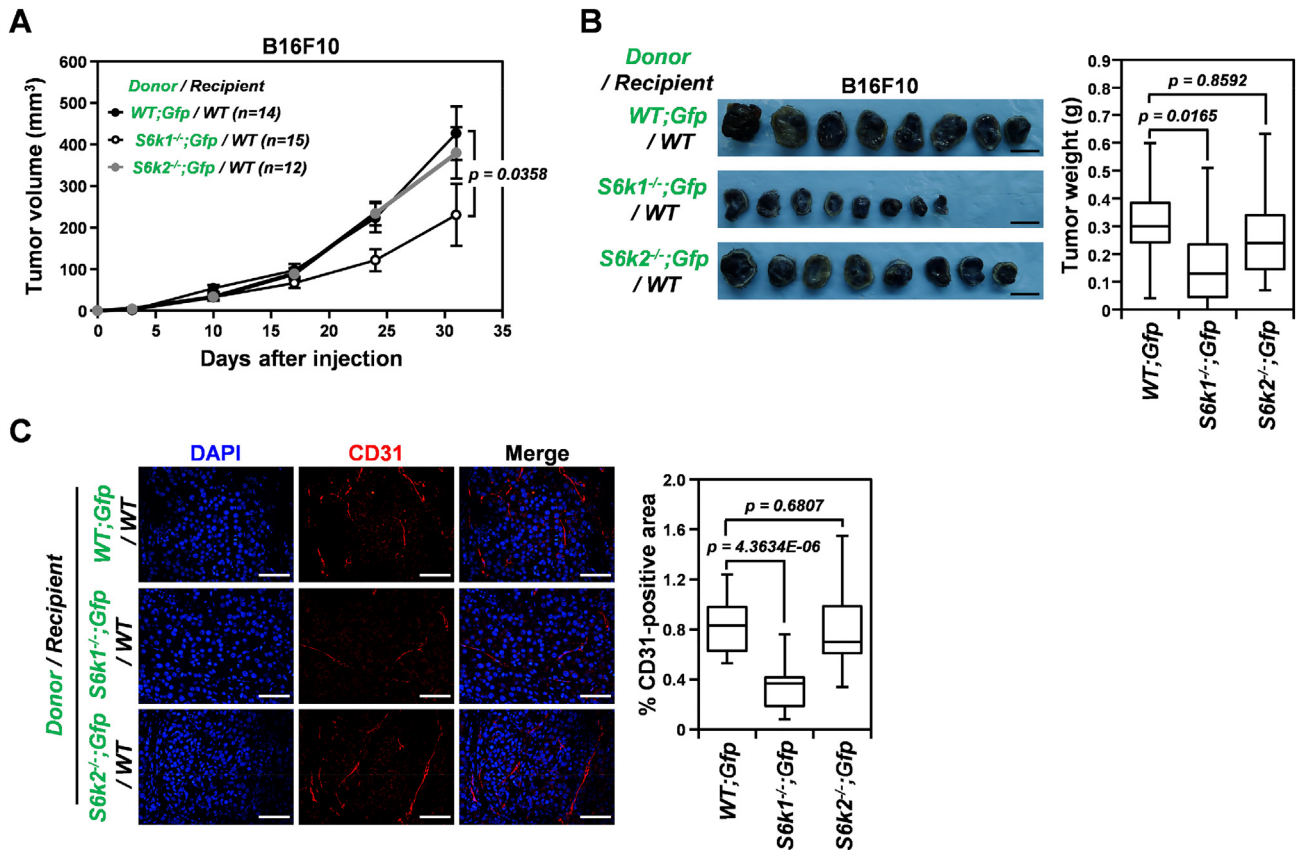


Figure 5. Reconstitution with $S6k1^{-/-}$ but not $S6k2^{-/-}$ bone marrow cells reduces the growth of B16F10 xenografts in wild-type recipient mice through attenuation of tumor angiogenesis. (A) Growth curves of B16F10 xenografts in wild-type recipient mice transplanted with bone marrow cells derived from $S6k1^{-/-}; Gfp$, $S6k2^{-/-}; Gfp$, or $WT; Gfp$ mice as a control. Data are presented as means \pm SEM. (B) Representative images (left panel) and weights (right panel) of B16F10 tumors harvested from recipient mice at 31 days after injection. Scale bars: 1 cm. Data are presented as box plots with medians and minimum to maximum whiskers. (C) Quantification of MVD in B16F10 xenografts isolated from recipient mice at 31 days postinjection. Scale bars: 50 μ m. Data are presented as box plots with medians and minimum to maximum whiskers.

S6K Isoforms Are Dispensable for the Recruitment of CD11b⁺Gr1^{hi} Myeloid-Derived Suppressor Cells to the Tumor as well as Bv8 Production

MDSCs, especially the granulocytic CD11b⁺Gr1^{high} MDSC population, promote tumor angiogenesis by expressing the proangiogenic factor Bv8, also called prokineticin-2 [31]. Therapeutic inhibition of mTOR signaling, however, has been shown to decrease intratumoral accumulation of MDSCs [32]. To determine whether the bone marrow-derived cell population was responsible for the defective angiogenic phenotype observed in $S6k1^{-/-}$ mice, we first investigated how loss of each S6K isoform affected the mobilization of CD11b⁺Gr1^{high} MDSCs into peripheral blood from the bone marrow and their recruitment to the tumor in mice bearing same-sized B16F10 and LLC tumor xenografts (Figure 6). Loss of either S6K1 or S6K2 had no significant effect on the percentage of circulating and tumor-infiltrating CD11b⁺Gr1^{high} MDSCs in bone marrow compared to wild-type controls in either B16F10 or LLC tumor-bearing mice (Figure 6, A-D). Although the number of tumor-infiltrating CD11b⁺Gr1^{high} MDSCs increased slightly in B16F10 tumor-bearing mice upon S6K2 loss compared to the wild-type control, this increase was not statistically significant ($P > .05$) (Figure 6B). Next, we examined the possibility of impaired Bv8 expression in CD11b⁺Gr1^{high} MDSCs upon S6K1 loss (Figure 6, E and F). In both B16F10 and LLC tumor xenografts, intratumoral Bv8 concentration measured by ELISA was not significantly different between $S6k1^{-/-}$ or $S6k2^{-/-}$ mice and wild-type mice. Although S6K1 loss seemed to slightly increase Bv8 expression in B16F10 tumors, this increase was not significant compared to wild-type controls ($P > .05$) (Figure 6E). These observations indicate that both S6K isoforms are dispensable for the mobilization and

recruitment of CD11b⁺Gr1^{high} MDSCs from the bone marrow to the tumor bed as well as Bv8 production by these MDSCs.

Taken together, our data suggest that CD11b⁺Gr1^{high} MDSCs are not the cellular factor involved in the attenuated tumor angiogenesis observed upon loss of S6K1 in the tumor microenvironment.

Loss of S6K1 Decreases Lactate-Induced VEGF Production in Bone Marrow-Derived Macrophages Without Affecting Their Infiltration and M2 Polarization in Tumors

TAMs, especially the M2-polarized subtype, have been demonstrated to promote tumor growth and progression by inducing the angiogenic switch in dormant tumors through VEGF production [33]. In addition, mTOR signaling has been shown to be essential for both differentiation of monocytes to M2-polarized macrophages and expression of VEGF in these polarized macrophages [34,35]. Therefore, we first investigated whether loss of S6K isoforms, especially S6K1, affected the number of TAMs and M2-polarized macrophages in B16F10 and LLC tumors implanted in $S6k1^{-/-}$, $S6k2^{-/-}$, and wild-type mice (Figure 7). The number of CD11b⁺F4/80⁺ macrophages measured by flow cytometry was not significantly different in B16F10 or LLC tumors derived from either $S6k1^{-/-}$ or $S6k2^{-/-}$ mice compared to those implanted in wild-type mice (Figure 7, A-D). In addition, the number of F4/80⁺ macrophages positive for CD206, a marker of the M2-polarized subtype, was unaltered in B16F10 xenografts implanted in either $S6k1^{-/-}$ or $S6k2^{-/-}$ mice compared to wild-type controls (Figure 7, A and B). In LLC xenografts, loss of S6K1 slightly reduced the number of CD206⁺F4/80⁺ macrophages compared to the wild-type

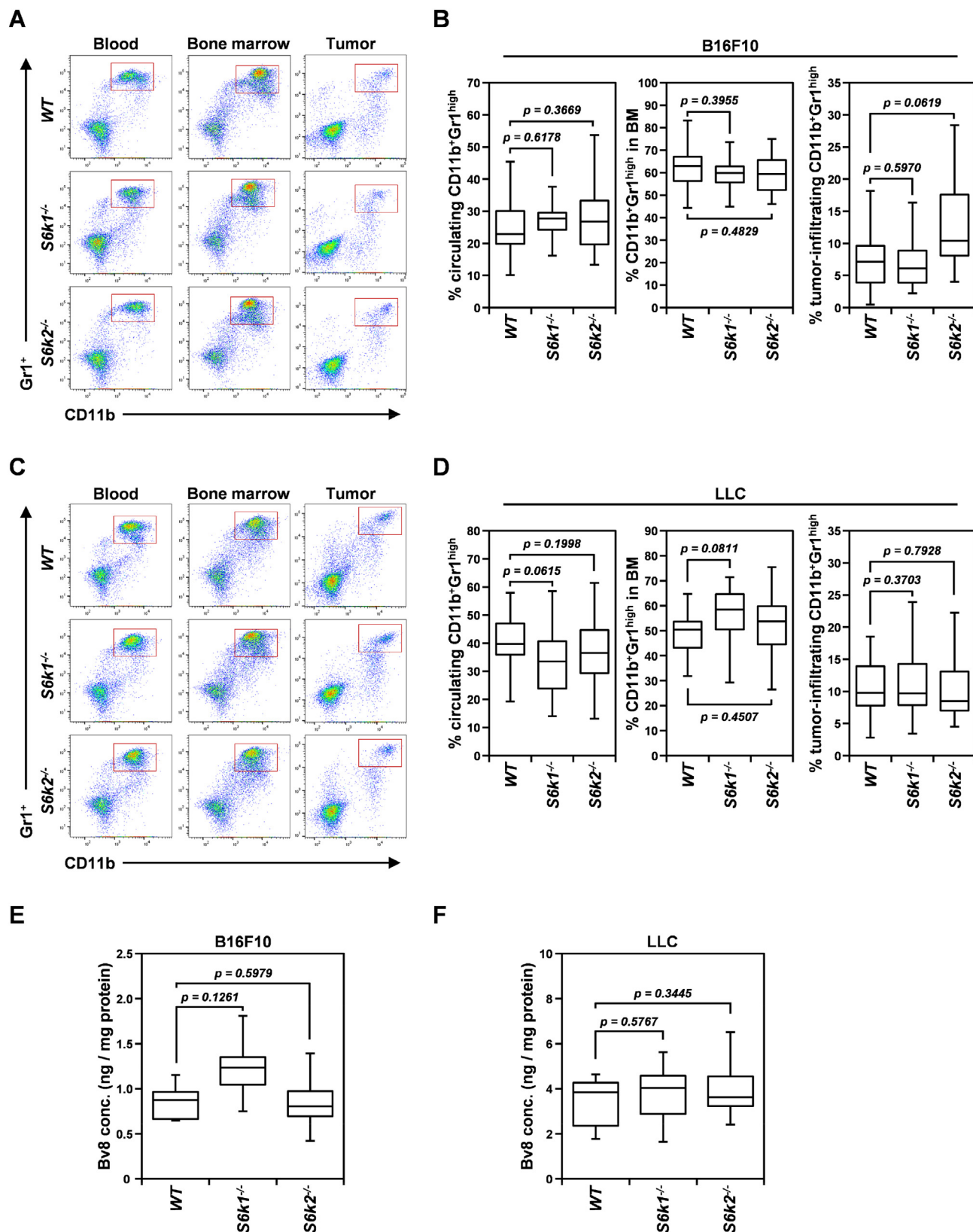


Figure 6. Inactivation of either *S6k1* or *S6k2* does not affect the frequency of CD11b⁺Gr1^{hi} myeloid-derived suppressor cells or their production of Bv8 in tumors. (A and B) Representative flow cytometry images (A) and quantification (B) of CD11b⁺Gr1^{hi} myeloid-derived suppressor cells (gated in red boxes) in the blood circulation, bone marrow (BM), and tumors in *S6k1*^{-/-} ($n = 11$), *S6k2*^{-/-} ($n = 16$), and wild-type ($n = 24$) mice bearing B16F10 xenografts of similar size. (C and D) Representative flow cytometry images (C) and quantification (D) of CD11b⁺Gr1^{hi} myeloid-derived suppressor cells in the blood circulation, BM, and tumors in *S6k1*^{-/-} ($n = 22$), *S6k2*^{-/-} ($n = 23$), and wild-type ($n = 24$) mice bearing LLC xenografts of similar size. (E and F) Intratumoral Bv8 concentration assessed by ELISA in B16F10 (E) and LLC (F) xenografts. Data are presented as box plots with medians and minimum to maximum whiskers.

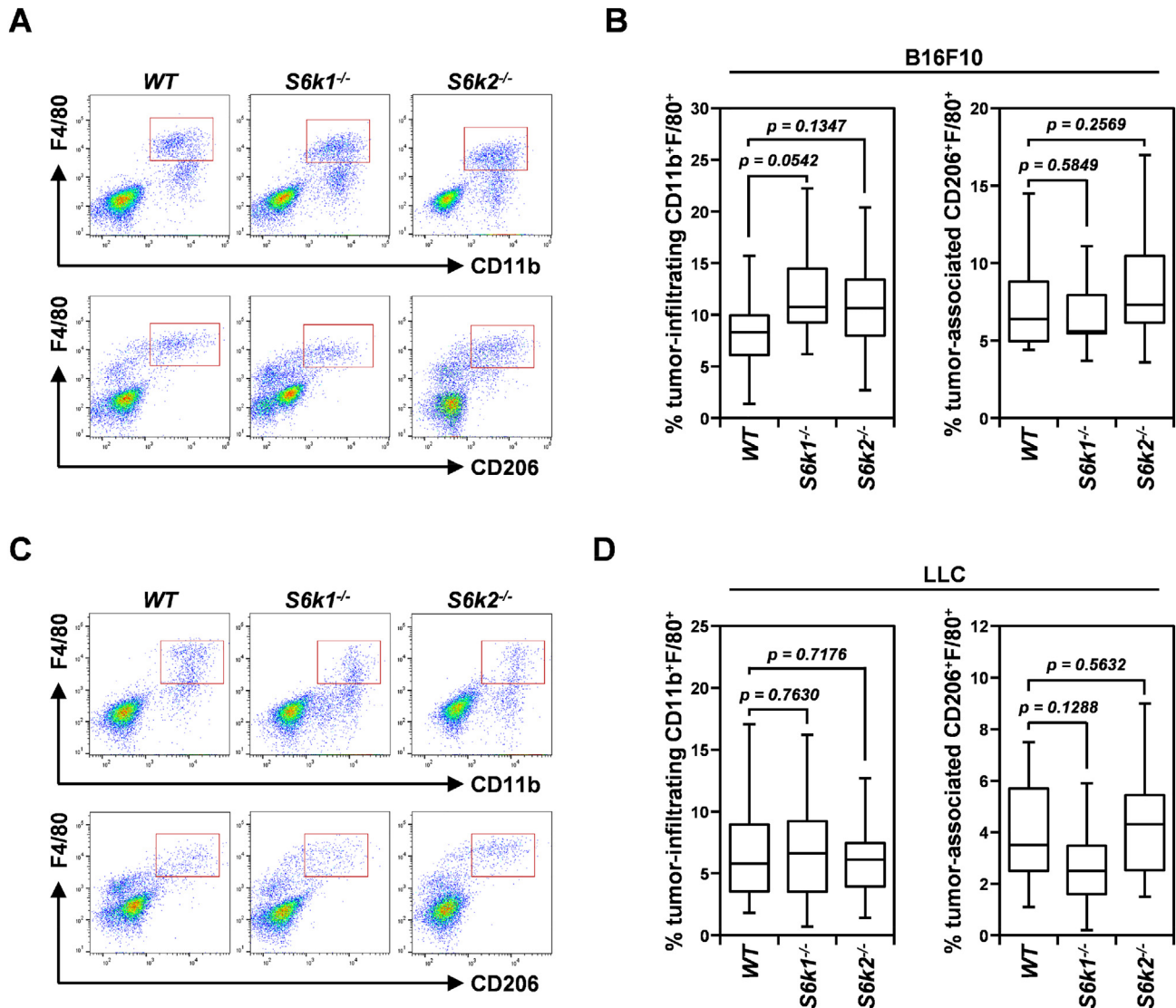


Figure 7. Loss of either S6K1 or S6K2 does not alter the number of TAMs or the frequency of M2-polarized macrophages in tumors. (A and B) Representative flow cytometry images (A) and quantification (B) of the number of CD11b⁺F4/80⁺ and CD206⁺F4/80⁺ macrophages (gated in red boxes) in similar-sized B16F10 xenografts from *S6k1*^{-/-} ($n = 12$), *S6k2*^{-/-} ($n = 14$), and wild-type ($n = 20$) mice. (C and D) Representative flow cytometry images (C) and quantification (D) of the number of CD11b⁺F4/80⁺ and CD206⁺F4/80⁺ macrophages in similar-sized LLC xenografts in *S6k1*^{-/-} ($n = 14$), *S6k2*^{-/-} ($n = 18$), and wild-type ($n = 13$) mice. Data are presented as box plots with medians and minimum to maximum whiskers.

control (Figure 7, C and D), but this decrease was not statistically significant ($P > .05$). These observations imply that the two S6K isoforms are not required for mTOR signaling-based recruitment of macrophages to the tumor bed or their differentiation into the M2-polarized subtype.

Through both transcriptional and translational control of HIF-1 α , a key transcription factor involved in VEGF expression, mTOR signaling mediates VEGF production in macrophages in response to various stimuli such as tumor-derived lactate and LPS, a Toll-like receptor 4 ligand [36,37]. Therefore, to examine whether S6K isoforms, especially S6K1, are required for VEGF expression in macrophages in a lactate-enriched tumor environment, BMDMs were isolated from *S6k1*^{-/-}, *S6k2*^{-/-}, and wild-type mice and assessed for lactate-induced VEGF production as well as the expression of both S6K isoforms (Figures 8 and S3). VEGF protein level measured by ELISA revealed that loss of S6K1 but not S6K2 dampened VEGF upregulation induced by lactate treatment compared to the wild-type control in BMDMs (Figure 8A). In addition, upon treatment with lactate, BMDMs from *S6k1*^{-/-} mice displayed an attenuated increase in *Vegf* mRNA compared to that observed in *S6k2*^{-/-} and wild-type mice (Figure 8B), suggesting that S6K1 loss affects VEGF upregulation in macrophages triggered by

lactate in a transcription-dependent manner. Indeed, loss of S6K1 was also found to impair VEGF upregulation in BMDMs elicited by combined treatment with LPS and NECA, an adenosine A2A receptor agonist, which are known to stimulate *Vegf* mRNA transcription by inducing *Hif-1 α* expression in macrophages [38] (Figure 8C).

Based on the fact that LPS and NECA upregulate *Hif-1 α* by inducing *Hif-1 α* gene transcription and stabilizing *Hif-1 α* mRNA, respectively [38], our results suggested that S6K1 contributes to lactate-induced VEGF production in BMDMs by increasing levels of HIF-1 α in a transcription-dependent manner. To verify that S6K1 is required for the induction of HIF-1 α in BMDMs upon exposure to lactate, we investigated whether loss of S6K1 attenuated HIF-1 α expression in BMDMs after stimulation with lactate (Figure 8, D and E). Four hours after treatment with lactate, as expected, S6K2 deficiency had no effect on the mRNA level of *Hif-1 α* in BMDMs compared with that in wild-type control cells (Figure 8D). However, *S6k1*^{-/-} BMDMs showed a significant reduction in *Hif-1 α* mRNA level by approximately 32% as compared to wild-type control cells. In addition, lactate-induced HIF-1 α protein expression assessed using immunoblotting was also found to be decreased in *S6k1*^{-/-} BMDMs by up to 46% and 44% compared to wild-type controls

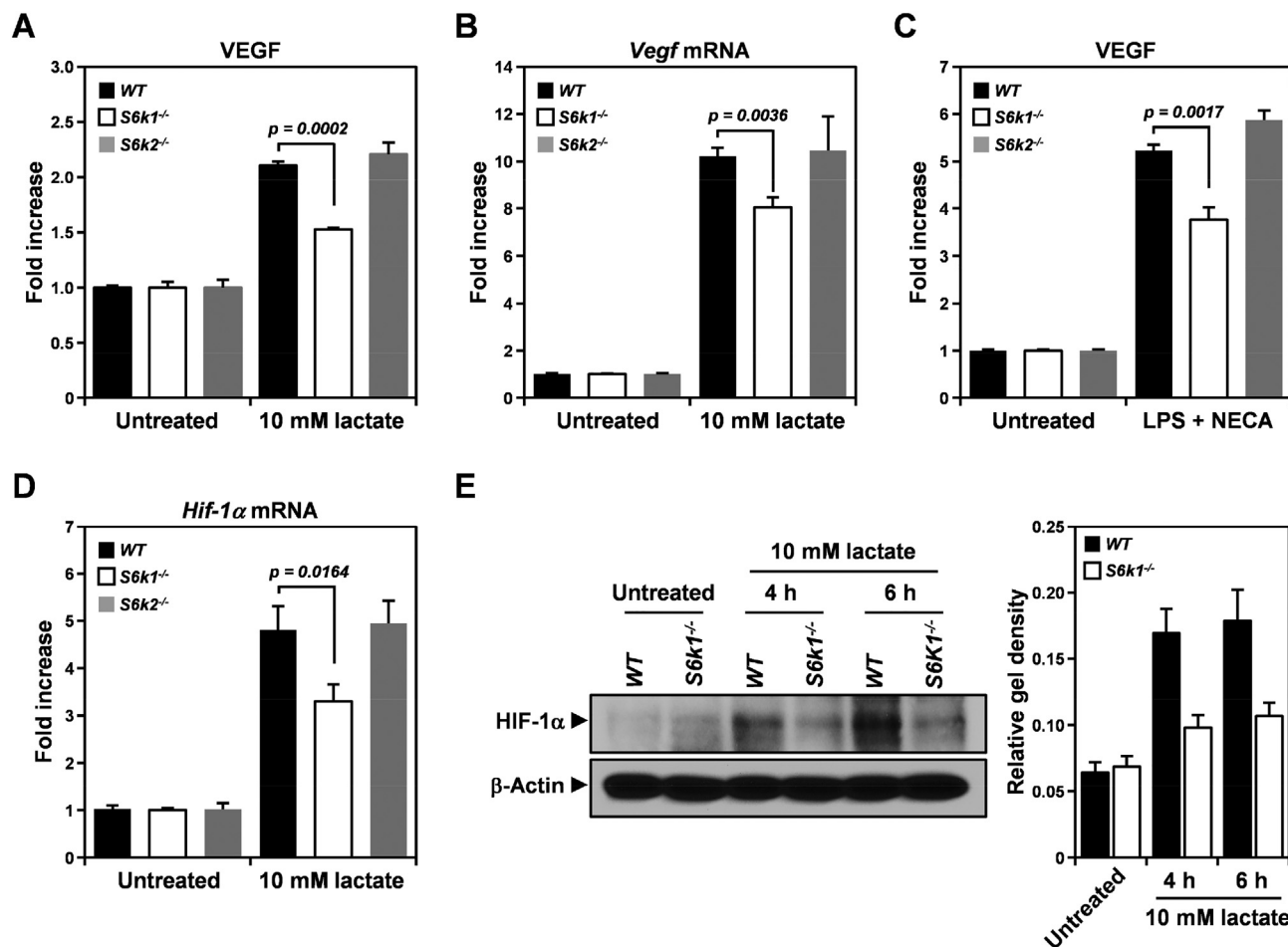


Figure 8. Deletion of *S6k1* but not *S6k2* attenuates lactate-induced VEGF production in bone marrow–derived macrophages. (A and B) Expression of VEGF protein detected using ELISA (A) and *Vegf* mRNA measured by real-time PCR in *S6k1*^{-/-}, *S6k2*^{-/-}, and wild-type bone marrow–derived macrophages after treatment with 10 mM lactate for 24 and 6 hours, respectively. (C) Level of VEGF protein assessed using ELISA in *S6k1*^{-/-}, *S6k2*^{-/-}, and wild-type bone marrow–derived macrophages after 24 hours of treatment with 100 μg/ml LPS combined with 1 μM NECA. (D) Level of *Hif-1α* mRNA measured by real-time PCR in *S6k1*^{-/-}, *S6k2*^{-/-}, and wild-type bone marrow–derived macrophages treated with 10 mM lactate for 4 hours. (E) HIF-1α protein level assessed by immunoblotting in *S6k1*^{-/-} and wild-type bone marrow–derived macrophages after treatment with 10 mM lactate for 4 and 6 hours. β-Actin served as a loading control, and relative gel density was determined by quantification with densitometry and analysis using ImageJ software. Data are presented as means ± SEM.

at 4 and 6 hours of treatment, respectively (Figure 8E). These observations suggest that the attenuated VEGF expression observed in *S6k1*^{-/-} BMDMs is attributable to a defect in HIF-1α induction triggered by lactate. In addition, together with previously published studies that have demonstrated mTOR-mediated HIF-1α expression [11,39], our results imply that S6K1 but not S6K2 is involved in downstream mTOR signaling, resulting in lactate-induced HIF-1α expression in BMDMs.

Overall, our data indicate that loss of S6K1 but not S6K2 causes a defect in VEGF production by attenuating *Hif-1α* activation in BMDMs upon exposure to lactate without affecting their recruitment to the tumor bed and differentiation into proangiogenic M2 subsets. Considering the essential role of TAM-derived VEGF in the angiogenic switch in tumors, our results suggest that the reduced tumor angiogenesis and growth observed in the S6K1-deficient tumor microenvironment are, at least in part, attributable to attenuated VEGF production by TAMs upon S6K1 loss.

Discussion

In mammalian cells, mTOR is a core component of the catalytic subunit of two distinct protein complexes, mTOR complex-1 (mTORC1) and -2 (mTORC2), depending on its binding partners, regulatory-associated protein of mTOR (Raptor) and rapamycin-insensitive companion of mTOR (Rictor), respectively [4]. While mTORC1 has been shown to regulate cell

growth and metabolism by mediating protein synthesis and activating metabolic transcription factors through phosphorylation of various downstream targets, including S6Ks, eukaryotic translation initiation factor 4E-binding protein 1, and Lipin-1, mTORC2 has been reported to contribute to cell proliferation and survival by activating targets such as Akt, also known as protein kinase B and protein kinase C [4], indicating that these two mTOR complexes mediate different biological processes by controlling distinct signaling circuits. In our present study, because systemic administration of mTORC1 inhibitors such as rapamycin and temsirolimus has been shown to suppress tumor growth by both tumor cell-intrinsic and tumor cell-extrinsic mechanisms [7], we investigated the role of downstream mTORC1 signaling with a special focus on the mTORC1-S6K axis in the tumor microenvironment. To limit the effect of disruption of the mTORC1-S6K signaling pathway in the tumor microenvironment, we adopted mice deficient for each S6K isoform and two different tumor xenograft models, B16F10 and LLC, with intact mTORC1-S6K signaling. Interestingly, *S6k1*^{-/-} but not *S6k2*^{-/-} mice exhibited significantly suppressed growth of implanted tumors, suggesting that S6K1 but not S6K2 is required to create tumor-promoting conditions in the microenvironment. In addition, similar to what has been observed for therapeutic inhibition of mTORC1 [28], tumor growth suppression in the S6K1-deficient tumor stroma was accompanied by reduced tumor angiogenesis, suggesting that the mTORC1-S6K1 signaling axis is required for mediating the

angiogenic process in the tumor bed and thus promoting tumor growth. Depletion of S6K2 in the tumor stroma had no observable effect on tumor angiogenesis in mice, implying that S6K2 is dispensable for establishing a proangiogenic tumor microenvironment. To the best of our knowledge, this is the first study to show the effects of systemic depletion of each S6K isoform from the tumor stroma on tumor growth and angiogenesis. Our study also provides additional experimental evidence for the different roles of S6K1 and S6K2 in tumorigenesis.

Endothelial cells are major players in tumor angiogenesis, and mTOR signaling is pivotal for mediating the angiogenic activation of endothelial cells by proangiogenic factor, manifested by cell proliferation, tube formation, and sprouting [7]. However, the role of downstream mTOR signaling in controlling the angiogenic function of endothelial cells remains controversial. Previously, it was reported that rapamycin had an inhibitory effect on endothelial cell activation triggered by proangiogenic factors and that this effect was partially reversed by a rapamycin-resistant S6K1 mutant [15,28]. In addition, suppression of S6K1 activity by a dominant-negative S6K1 mutant was shown to modestly reduce the capacity of human dermal microvascular endothelial cells to promote tumor growth and angiogenesis in human prostate cancer cell-containing Matrigel plugs implanted in chicken chorioallantoic membranes [16]. By contrast, recent studies have demonstrated that inhibition of mTORC2 by Rictor depletion but not that of mTORC1 by either Raptor depletion or rapamycin treatment profoundly abrogated cell proliferation, migration, tube formation, and angiogenic sprouting in mouse and human endothelial cells *in vitro* as well as angiogenesis *in vivo* [40,41]. In addition, conditional deletion of the *Rictor* gene in mice was shown to significantly reduce the growth of LLC xenografts by attenuating tumor angiogenesis [41]. In parallel with these recent studies, we observed no significant alterations in angiogenic behaviors in primary endothelial cells upon loss of each S6K isoform *in vitro* and *in vivo*, further supporting the notion that mTORC1 signaling, especially the mTORC1-S6K axis, is not essential for mediating the angiogenic activation of endothelial cells in the tumor microenvironment. The discrepancy between study findings is presumably due to differential compensation by alternative signaling pathways in different experimental or environmental contexts. Indeed, sustained inhibition of mTORC1 activity by Raptor depletion or rapamycin was shown to decrease S6K1 phosphorylation but increase phosphorylation and activation of Akt1 and protein kinase C α by mTORC2, leading to vascular assembly and endothelial cell proliferation, respectively [40,41]. In addition, phosphorylation of S6, a major downstream target of the mTORC1-S6K signaling axis, was found to be maintained by mitogen-activated protein kinase-dependent kinase, most likely p90 ribosomal S6 kinase, in *S6k1*^{-/-};*S6k2*^{-/-} mouse embryonic fibroblasts [17]. Furthermore, rapamycin administration to rats undergoing kainite-induced seizure was observed to have distinct effects on S6 phosphorylation depending on the time of administration [42].

Interleukin-17 derived from tumor cells and tumor-infiltrating T helper type 17 cells stimulates secretion of granulocyte colony-stimulating factor (G-CSF) by TAFs and thus recruits bone marrow-derived cells, including MDSCs and macrophages, from the bone marrow to the tumor bed [25]. In addition, inhibition of mTORC1 has been shown to interfere with intratumoral accumulation of bone marrow-derived cells, especially MDSCs, by reducing the G-CSF level in the tumor bed [32]. In our study, reconstitution with S6K1-deficient bone marrow cells was found to reduce tumor growth and angiogenesis in wild-type recipients, indicating that S6K1 is required to mediate the tumor-promoting function of BMDMs. However, depletion of either S6K1 or S6K2 did not alter the frequency of tumor-infiltrating CD11b⁺Gr1^{high} MDSCs and macrophages, suggesting that the mTORC1-S6K axis is dispensable for mediating the interleukin-17-G-CSF signaling cascade.

Of interest, while loss of S6K1 did not affect Bv8 production by CD11b⁺Gr1^{high} MDSCs in tumors, S6K1-deficient BMDMs exhibited impaired VEGF production in response to stimulation with lactate, which is known to be enriched in the tumor bed and to induce VEGF expression in TAMs. Previous studies have shown that TAM-derived VEGF is critical for the angiogenic switch in tumor progression [33]. Hence, it is likely that

the reduced VEGF production by macrophages upon *S6k1* inactivation delayed the angiogenic switch in tumors, resulting in tumor growth suppression in *S6k1*^{-/-} mice. Growth of B16F10 and LLC xenografts in *S6k1*^{-/-} mice was not completely inhibited during the time period monitored; rather, tumors eventually started growing rapidly after 17 and 20 days, respectively, postinjection in those mice, while tumor growth in wild-type mice became exponential at 13 and 15 days, respectively, after injection. This delayed switch from linear to exponential growth of tumors observed in *S6k1*^{-/-} mice is similar to the retarded growth of dormant tumors seen in a model of human tumor dormancy until the angiogenic switch [43].

In our study, *S6k1*^{-/-} BMDMs displayed significant attenuation of both *Hif-1 α* mRNA and protein upregulation triggered by lactate. Together with previous findings showing that tumor-derived lactate upregulates VEGF expression in TAMs in an HIF-1 α -dependent fashion and that mTORC1 drives *Hif-1 α* expression in both a transcription- and translation-dependent manner [11,36,39], our results suggest that, upon exposure to lactate, S6K1 mediates downstream mTORC1 signaling to induce *Hif-1 α* expression in BMDMs. Impaired VEGF production in *S6k1*^{-/-} BMDMs can be attributed to compromised *Hif-1 α* transcription in those cells. Recently, S6K1 has been shown to participate in transcriptional control of gene expression both directly, through phosphorylation of histone H2B followed by enhancer of zeste homolog 2-mediated histone H3 trimethylation, and indirectly, via phosphorylation-mediated activation of transcription factors such as sterol regulatory element binding proteins [11,12]. In addition, S6K1 depletion was reported to reduce HIF-1 α expression induced by mTORC1 activation without affecting translation from *Hif-1 α* 5'UTR in mouse embryonic fibroblasts. Therefore, although further verification of whether S6K1 is dispensable for *Hif-1 α* mRNA translation mediated by mTORC1 signaling in BMDMs is needed, it is likely that S6K1 mediates mTORC1-driven *Hif-1 α* expression in a transcription-dependent but not translation-dependent manner in BMDMs.

Overall, we demonstrated that S6K1 but not S6K2 is crucial for establishing a microenvironment that favors tumor growth by mediating the proangiogenic function of bone marrow-derived cells. We also found that S6K1 is required for lactate-induced VEGF production in BMDMs by upregulating *Hif-1 α* expression. Although further investigation is still necessary to determine the role of S6K1 in mTOR-mediated immunosuppression of tumor-infiltrating bone marrow-derived cells, such as regulatory T cells and MDSCs, our findings provide important insight into the role of the mTORC1-S6K signaling axis in the tumor microenvironment. In addition, because S6Ks are considered potential targets for cancer treatment [8], our results have clinical implications.

Acknowledgements

We thank Dr. Sara Kozma and Dr. George Thomas for providing *S6k1*^{-/-} and *S6k2*^{-/-} mice. We thank Dr. Jae Hyeon Kim for providing *Gfp* mice. We are grateful to Dr. Sandra Ryeom for providing the LLC cell line and helpful discussion. This work was supported by a grant from the Basic Science Research Program through the National Research Foundation of Korea (NRF) funded by the Ministry of Education (NRF-2013R1A1A2058845) to K. H. B., a grant from the 2016 Basic-Clinical Collaborative Research Program funded by Samsung Biomedical Research Institute (SMX1161461) to K. H. B. and H. S. J., and a grant from the NRF-2015-Global PhD Fellowship Program of the National Research Foundation of Korea (NRF) funded by the Korean Government (NRF-2015H1A2A1034135) to S.L.

Declaration of Competing Interest

The authors have no conflicts of interest to declare.

Appendix A. Supplementary Data

Supplementary data to this article can be found online at <https://doi.org/10.1016/j.tranon.2020.100767>.

References

- [1] M Wang, J Zhao, L Zhang, F Wei, Y Lian, Y Wu, Z Gong, S Zhang, J Zhou, K Cao, et al., Role of tumor microenvironment in tumorigenesis, *J. Cancer* 8 (2017) 761–773.
- [2] DC Hinshaw, LA Shevde, The tumor microenvironment innately modulates cancer progression, *Cancer Res.* 79 (2019) 4557–4566.
- [3] M De Palma, D Biziato, TV Petrova, Microenvironmental regulation of tumour angiogenesis, *Nat. Rev. Cancer* 17 (2017) 457–474.
- [4] RA Saxton, DM Sabatini, mTOR signaling in growth, metabolism, and disease, *Cell* 169 (2017) 361–371.
- [5] DA Fruman, C Rommel, PI3K and cancer: lessons, challenges and opportunities, *Nat. Rev. Drug Discov.* 13 (2014) 140–156.
- [6] D Mossmann, S Park, MN Hall, mTOR signalling and cellular metabolism are mutual determinants in cancer, *Nat. Rev. Cancer* 18 (2018) 744–757.
- [7] F Conciatori, C Bazzichetto, I Falcone, S Pilotto, E Bria, F Cognetti, M Milella, L Ciuffreda, Role of mTOR signaling in tumor microenvironment: An overview, *Int. J. Mol. Sci.* 19 (2018) pii: E2453.
- [8] TR Fenton, IT Gout, Functions and regulation of the 70 kDa ribosomal S6 kinases, *Int. J. Biochem. Cell. Biol.* 43 (2011) 47–59.
- [9] AM Robitaille, S Christen, M Shimobayashi, M Cornu, LL Fava, S Moes, C Prescianotto-Baschong, U Sauer, P Jenoe, MN Hall, Quantitative phosphoproteomics reveal mTORC1 activates de novo pyrimidine synthesis, *Science* 339 (2013) 1320–1323.
- [10] I Ben-Sahra, JJ Howell, JM Asara, BD Manning, Stimulation of de novo pyrimidine synthesis by growth signaling through mTOR and S6K1, *Science* 339 (2013) 1323–1328.
- [11] K Duvel, JL Yecies, S Menon, P Raman, AI Lipovsky, AL Souza, E Triantafellow, Q Ma, R Gorski, S Cleaver, et al., Activation of a metabolic gene regulatory network downstream of mTOR complex 1, *Mol. Cell* 39 (2010) 171–183.
- [12] SA Yi, SH Um, J Lee, JH Yoo, SY Bang, EK Park, MG Lee, KH Nam, YJ Jeon, JW Park, et al., S6K1 phosphorylation of H2B mediates EZH2 trimethylation of H3: A determinant of early adipogenesis, *Mol. Cell* 62 (2016) 443–452.
- [13] K Kim, S Pyo, SH Um, S6 kinase 2 deficiency enhances ketone body production and increases peroxisome proliferator-activated receptor alpha activity in the liver, *Hepatology* 55 (2012) 1727–1737.
- [14] HMS Ismail, Downstream the mTOR: S6 kinases between divergence and redundancy, *J. Biochem. Pharmacol. Res.* 1 (2013) 94–105.
- [15] F Viñals, JC Chambard, J Poysségur, J. p70 S6 kinase-mediated protein synthesis is a critical step for vascular endothelial cell proliferation, *J. Biol. Chem.* 274 (1999) 26776–26782.
- [16] LZ Liu, JZ Zheng, XR Wang, BH Jiang, Endothelial p70 S6 kinase 1 in regulating tumor angiogenesis, *Cancer Res.* 68 (2008) 8183–8188.
- [17] M Pende, SH Um, V Mieulet, M Sticker, VL Goss, J Mestan, M Mueller, S Fumagalli, SC Kozma, G Thomas, *S6K1^{-/-}/S6K2^{-/-}* mice exhibit perinatal lethality and rapamycin-sensitive 5'-terminal oligopyrimidine mRNA translation and reveal a mitogen-activated protein kinase-dependent S6 kinase pathway, *Mol. Cell. Biol.* 24 (2004) 3112–3124.
- [18] S Alliouachene, RL Tuttle, S Boumard, T Lapointe, S Berissi, S Germain, F Jaubert, D Tosh, MJ Birnbaum, M Pende, Constitutively active Akt1 expression in mouse pancreas requires S6 kinase 1 for insulinoma formation, *J. Clin. Invest.* 118 (2008) 3629–3638.
- [19] H Shima, M Pende, Y Chen, S Fumagalli, G Thomas, SC Kozma, Disruption of the *p70^{s6k}/p85^{s6k}* gene reveals a small mouse phenotype and a new functional S6 kinase, *EMBO J.* 17 (1998) 6649–6659.
- [20] M Okabe, M Ikawa, K Kominami, T Nakanishi, Y Nishimune, Y. 'Green mice' as a source of ubiquitous green cells, *FEBS Lett.* 407 (1997) 313–319.
- [21] MS O'Reilly, T Boehm, Y Shing, N Fukai, G Vasios, WS Lane, E Flynn, JR Birkhead, BR Olsen, J Folkman, Endostatin: an endogenous inhibitor of angiogenesis and tumor growth, *Cell* 88 (1997) 277–285.
- [22] J Shin, JC Lee, KH Baek, A single extra copy of *Dscr1* improves survival of mice developing spontaneous lung tumors through suppression of tumor angiogenesis, *Cancer Lett.* 342 (2014) 70–81.
- [23] JI Virag, CE Murry, Myofibroblast and endothelial cell proliferation during murine myocardial infarct repair, *Am. J. Pathol.* 163 (2003) 2433–2440.
- [24] YZ Cui, H Hisha, GX Yang, TX Fan, T Jin, Q Li, Z Lian, S Ikehara, S. Optimal protocol for total body irradiation for allogeneic bone marrow transplantation in mice, *Bone Marrow Transplant* 30 (2002) 843–849.
- [25] AS Chung, X Wu, G Zhuang, H Ngu, I Kasman, J Zhang, JM Vernes, Z Jiang, YG Meng, FV Peale, et al., An interleukin-17-mediated paracrine network promotes tumor resistance to anti-angiogenic therapy, *Nat. Med.* 19 (2013) 1114–1123.
- [26] J Weischenfeldt, B Porse, Bone marrow-derived macrophages (BMM), isolation and applications, *Cold Spring Harb. Protoc.* (2008) <https://doi.org/10.1101/pdb.prot5080>.
- [27] F Heidebrecht, A Heidebrecht, I Schulz, SE Behrens, A Bader, Improved semiquantitative Western blot technique with increased quantitative range, *J. Immunol. Methods* 345 (2009) 40–48.
- [28] M Guba, P von Breitenbuch, M Steinbauer, G Koehl, S Flegel, M Hornung, CJ Bruns, C Zuelke, S Farkas, M Anthuber, et al., Rapamycin inhibits primary and metastatic tumor growth by antiangiogenesis: involvement of vascular endothelial growth factor, *Nat. Med.* 8 (2002) 128–135.
- [29] A Raza, MJ Franklin, AZ Dudek, Pericytes and vessel maturation during tumor angiogenesis and metastasis, *Am. J. Hematol.* 85 (2010) 593–598.
- [30] D Keskin, J Kim, VG Cooke, CC Wu, H Sugimoto, C Gu, M De Palma, R Kalluri, VS LeBleu, Targeting vascular pericytes in hypoxic tumors increases lung metastasis via angiopoietin-2, *Cell Rep.* 10 (2015) 1066–1081.
- [31] F Shojaei, X Wu, C Zhong, L Yu, XH Liang, J Yao, D Blanchard, C Bais, FV Peale, N van Bruggen, et al., Bv8 regulates myeloid-cell-dependent tumour angiogenesis, *Nature* 450 (2007) 825–831.
- [32] T Welte, IS Kim, L Tian, X Gao, H Wang, J Li, XB Holdman, JI Herschkowitz, A Pond, G Xie, et al., Oncogenic mTOR signalling recruits myeloid-derived suppressor cells to promote tumour initiation, *Nat. Cell Biol.* 18 (2016) 632–644.
- [33] V Riabov, A Gudima, N Wang, A Mickle, A Orekhov, J Kzhyshkowska, Role of tumor associated macrophages in tumor angiogenesis and lymphangiogenesis, *Front. Physiol.* 5 (2014) <https://doi.org/10.3389/fphys.2014.00075>.
- [34] V Byles, AJ Covarrubias, I Ben-Sahra, DW Lamming, DM Sabatini, BD Manning, T Horng, The TSC-mTOR pathway regulates macrophage polarization, *Nat. Commun.* 4 (2013) <https://doi.org/10.1038/ncomms3834>.
- [35] W Chen, T Ma, XN Shen, XF Xia, GD Xu, XL Bai, TB Liang, Macrophage-induced tumor angiogenesis is regulated by the TSC2-mTOR pathway, *Cancer Res.* 72 (2012) 1363–1372.
- [36] OR Colegio, NQ Chu, AL Szabo, T Chu, AM Rhebergen, V Jairam, N Cyrus, CE Brokowski, SC Eisenbarth, GM Phillips, et al., Functional polarization of tumour-associated macrophages by tumour-derived lactic acid, *Nature* 513 (2014) 559–563.
- [37] CC Blouin, EL Pagé, GM Soucy, DE Richard, Hypoxic gene activation by lipopolysaccharide in macrophages: implication of hypoxia-inducible factor 1alpha, *Blood* 103 (2004) 1124–1130.
- [38] M Ramanathan, G Pinhal-Enfield, I Hao, SJ Leibovich, Synergistic up-regulation of vascular endothelial growth factor (VEGF) expression in macrophages by adenosine A2A receptor agonists and endotoxin involves transcriptional regulation via the hypoxia response element in the VEGF promoter, *Mol. Biol. Cell* 18 (2007) 14–23.
- [39] KM Dodd, J Yang, MH Shen, JR Sampson, AR Tee, mTORC1 drives HIF-1α and VEGF-A signalling via multiple mechanisms involving 4E-BP1, S6K1 and STAT3, *Oncogene* 34 (2015) 2239–2250.
- [40] MA Farhan, K Carmine-Simmen, JD Lewis, RB Moore, AG Murray, Endothelial cell mTOR complex-2 regulates sprouting angiogenesis, *PLoS One* 10 (2015), e0135245.
- [41] S Wang, KR Amato, W Song, V Youngblood, K Lee, M Boothby, DM Brantley-Sieders, J Chen, Regulation of endothelial cell proliferation and vascular assembly through distinct mTORC2 signaling pathways, *Mol. Cell. Biol.* 35 (2015) 1299–1313.
- [42] L Chen, L Hu, JY Dong, Q Ye, N Hua, M Wong, LH Zeng, Rapamycin has paradoxical effects on S6 phosphorylation in rats with and without seizures, *Epilepsia* 53 (2012) 2026–2033.
- [43] GN Naumov, E Bender, D Zurakowski, SY Kang, D Sampson, E Flynn, RS Watnick, O Straume, LA Akslen, J Folkman, et al., A model of human tumor dormancy: an angiogenic switch from the nonangiogenic phenotype, *J. Natl. Cancer Inst.* 98 (2006) 316–325.